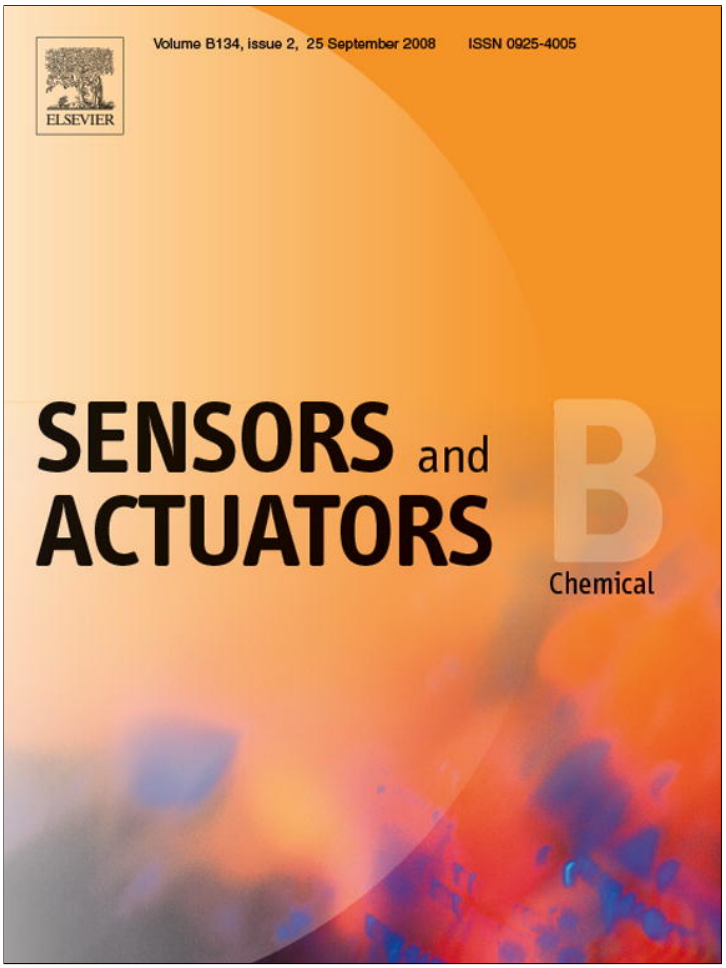

Sensors and Actuators B 134 (2008) 367–372

Contents lists available at ScienceDirect

Sensors and Actuators B: Chemical

journal homepage: www.elsevier.com/locate/snb

Electrochemical and photoelectrical properties of titania nanotube arrays annealed in different gases

Peng Xiao[a,b], Dawei Liu[b], Betzaida Batalla Garcia[b], Saghar Sepehri[b], Yunhuai Zhang[c], Guozhong Cao[b,*]

[a] Physics Department, Chongqing University, Chongqing 400044, PR China
[b] Department of Materials Science & Engineering, University of Washington, Seattle, WA 98195, USA
[c] Department of Chemical Engineering, Chongqing University, Chongqing 400044, PR China

ARTICLE INFO

Article history:
Received 15 February 2008
Accepted 7 May 2008
Available online 14 May 2008

Keywords:
Titania nanotubes arrays
Calcination
Conductivity
Electrochemical property
Photocurrent

ABSTRACT

Titania nanotube arrays fabricated by anodic oxidation of titanium foil were calcined in dry nitrogen, air, and argon at various temperatures for varied period of time. Changes in morphology and crystallinity of the nanotube arrays were studied by means of SEM and XRD. The influences of annealing conditions on the electrochemical and conductivity were investigated by electrochemical impedance spectroscopy (EIS), and the results showed that the electrical conductivities of TiO_2 nanotube arrays calcined in nitrogen for 3 h were improved greatly as compared to the as-grown titania nanotube arrays or annealed in air or argon. Well defined oxidation and reduction peaks were observed during the cyclic voltammetric scan at 0.1 V/s in 10 mM $K_3[Fe(CN)_6]$ solution. Photocurrent response in TiO_2 nanotube arrays calcined in nitrogen was significantly enhanced. Reduction of tetravalent titanium cations and the formation of oxygen vacancies were ascribed to explain the improved electrochemical and photoelectrical properties of titania nanotube arrays.

1. Introduction

Titania nanotube (TNT) arrays have attracted much attention because of their large specific surface area, favorable surface chemistry, and good biocompatibility [1–5]. For example, the surface chemistry of TNT can be easily modified through coordination with amine and carboxyl groups, and used in detection of electroactive molecules or as biosensors [6–9]. There are three general approaches to the synthesis of TiO_2 nanotubular structures, namely, template-assisted fabrication [10,11], alkaline hydrothermal synthesis [12], and anodic oxidation or anodization of titanium [13]. The advantage of TiO_2 nanotubes produced by anodization is that they are readily attached onto a titanium substrate and form oriented, aligned perpendicular to the substrate, which offers much improved electron transfer pathways than non-oriented (random mixtures) structure. As a result, this oriented TiO_2 nanotubes has a great potential as electrochemical electrodes for highly sensitive (bio)sensor applications. However, an obstacle preventing TNT arrays from wide spread applications is their irreversible electrode reactions. Reduction peaks were commonly observed, but no oxidative peaks can be seen in the reverse potential scan during the cyclic voltammetric measurements due to the low electrical conductivity of titania [14,15]. Calcination in different gases and doping are considered to be one viable approach to narrow the band gap and enhance the electrical conductivity [16–20]. However, most of the research was focused on nanocrystalline TiO_2 for applications of dye-sensitized solar cells.

In the present paper, we report the electrochemical characterization, conductivity and photocurrent response of TNT arrays annealed in N_2, Ar and air, respectively. The experimental results revealed the presence of both oxidation and reduction peaks of TNT electrode annealed in N_2 during the cyclic voltammetric tests. The electrochemical impedance spectroscopy (EIS) measurements also showed that the electrical conductivity of TNT annealed in N_2 increased significantly, and the relationship between the annealing and electrochemical and photoelectrical properties is discussed.

2. Experimental

Titania nanotube arrays were synthesized by means of anodic oxidation in electrolyte solution according to the method reported in literature [21]. Titanium foil (99% pure, 0.5-mm thick), potassium fluoride (KF, 99%), sodium hydrogen sulfate ($NaHSO_4$, 98%) and citric acid ($C_6O_7H_8{\cdot}H_2O$, 100%) were purchased from VWR. The titanium foils were ultrasonically cleaned in 18% HCl solution, followed

* Corresponding author. Tel.: +1 2066169084; fax: +1 2065433100.
E-mail addresses: xp6510@hotmail.com (P. Xiao), gzcao@u.washington.edu (G. Cao).

0925-4005/$ – see front matter © 2008 Elsevier B.V. All rights reserved.
doi:10.1016/j.snb.2008.05.005

by distilled water and acetone ultrasonic rinse prior to anodization. The electrolyte was composed of 0.1 M KF, 1.0 M $NaHSO_4$, and 0.2 M critric acid, sodium hydroxide was added to adjust the pH value to ~4 as measured with a pH meter (Model 3000, VWR scientific). The anodization was conducted in a two-electrode cell with a platinum foil as cathode at a constant potential of 22 V.

The as-grown TNT arrays were calcined at temperatures ranging from 300 to 650 °C in tube furnace, under a flow of dry N_2, with a heating rate of 4 °C/min and dwelled time between 1 and 6 h, similar to the conditions used in the literature [22]. In order to compare with the effects of calcination in nitrogen, the as-grown TNT was also calcined in air and argon at the same temperatures, respectively. The resultant TNT arrays are hereinafter designated as: TNT/N_2, for nitrogen-calcination, TNT/Ar, for argon-calcination and TNT/air, for air-calcination.

The surface morphology of the TiO_2 nanotubes before and after calcination was characterized by scanning electron microscope (SEM, Philips, JEOL JSM7000). X-ray diffraction (XRD) patterns were recorded using a Philips 1820 X-ray diffractometer with Cu Kα radiation (λ = 1.5418 Å) for understanding the crystallization and evolution of different phases as a function of calcination temperatures. EIS measurements were carried out in a Salon 1260 impedance/gain-phase analyzer and electrochemical software Z-plot was employed for impedance data analyses. A Pt foil and Ag/AgCl electrode were used as the counter electrode and reference electrode. The amplitude of the modulation potential for EIS measurement was 10 mV, the range of the frequency was from 400 kHz to 0.05 Hz. The electrochemical properties of the TNT electrodes were monitored using CV in 1 M KCl solution at 0.1 V/s in the presents of 10 mM $K_3[Fe(CN)_6]$ by an electrochemical workstation (CHI6051C). The photocurrent response was measured in 0.01 M Na_2SO_4 under the radiation of 0.16AMPS UV illumination (Mineralight Lamp UVGL-58) in the range of 366 nm at a potential of 1.5 V (Ag/AgCl).

3. Results and discussion

3.1. Structural characterization of TNT arrays

Fig. 1 shows the morphology SEM images of TNT before calcination (a), after calcination in N_2 at 300 °C for 3 h (b), 500 °C for 3 h (c) and for 6 h (d). The average diameter and wall thick-

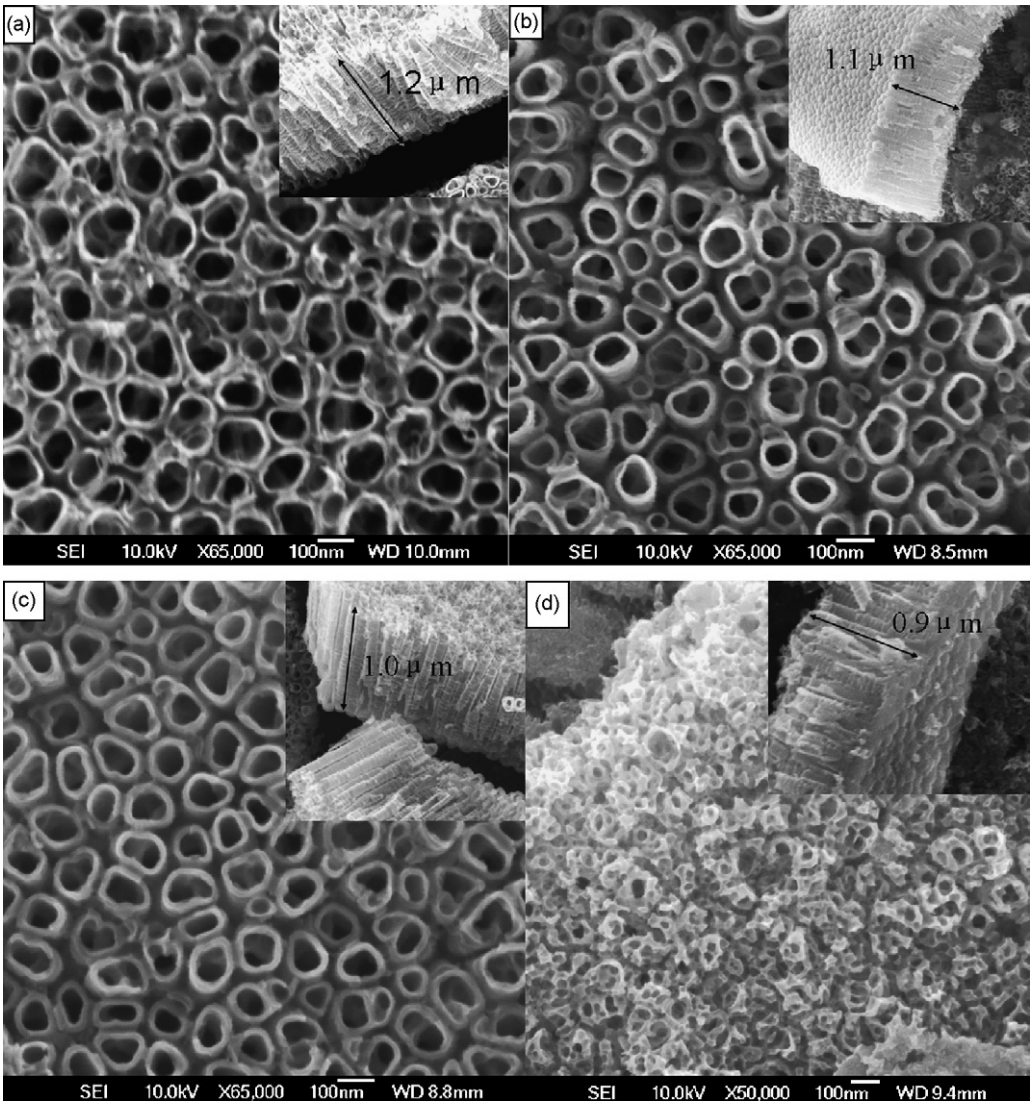

Fig. 1. SEM images of TiO_2 nanotubes (a) before calcinations, (b) calcined in N_2 at 300 °C for 3 h, (c) calcined in N_2 at 500 for 3 h, (d) calcined in N_2 at 500 °C for 6 h.

ness of TNT were estimated from the SEM images and averaged over a large area. Prior to calcination, the TNT has an inner diameter of ~100 nm and wall thickness ~9 nm, the length of the tube is 1.2 μm. After calcined at 300 °C and 500 °C for 3 hrs, the inner diameters decreased to 90 nm and 78 nm, while the wall thickness increased to 14 nm and 20 nm, and the length decreased to 1.1 μm and 1.0 μm, respectively. A prolonged annealing at 500 °C in N_2 for 6 h resulted in the collapse of TNT arrays. The wall thickness increased to 30 nm with most of the nanotube wall stuck together and the length of the tube decreased to 0.9 μm. These results indicate significant sintering of TNT arrays occurred during calcinations at temperatures above 300 °C. As expected, the increase of wall thickness was accompanied with a decrease in the length of TNT according to SEM cross-section images. Such a change of morphology is thermodynamically favorable, as it results in a reduction of specific surface area and thus the total surface energy. Nanostructures or nanomaterials, possessing large specific surface area and thus surface energy, are thermodynamically metastable [23], and would change their morphologies under favorable conditions. At elevated temperatures, high surface area makes them prone to solid-state sintering, which leads to grain growth, densification, and the increase of wall thickness. Since sintering is an activated process involving mass transfer [24], a higher annealing temperature or a prolonged annealing time favors more sintering and tends to destroy nanostructures completely. It should be noted that similar morphology change was observed when TNT arrays were calcined in argon under otherwise the same conditions. However, when calcined in air, TNT morphology is more stable and will only be destroyed when fired at 500 °C for over 9 h. When the as-prepared nanotubes were calcined in different gases for 3 h, the color of the samples changed, from gray green for the as-prepared TNT, to the gray yellow for the TNT/air, to gray blue for TNT/Ar and to dark blue for TNT/N_2.

Fig. 2 are the XRD patterns of TNT arrays calcined in N_2 for 3 h at different temperatures. Crystallization in amorphous TNT arrays (as-grown TNT) occurred at a temperature as low as 300 °C. The XRD peaks of anatase phase are unambiguously visible, indicating the phase transition from amorphous to anatase crystal. Heating at higher temperatures such as 650 °C, resulted in the formation of rutile phase. The phase formation and transition temperatures observed in this work are in a good agreement with the literature data [25,26]. In spite of some trivial differences when annealed at higher temperatures, the TNT arrays calcinated at 500 °C for 3 h possess similar morphology and XRD patterns regardless the annealing gas atmospheres.

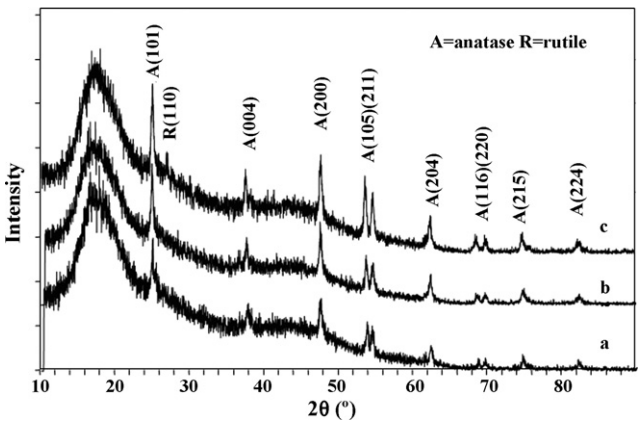

Fig. 2. XRD pattern of titania nanotube arrays calcined in N_2 at (a) 300 °C, (b) 500 °C, and (c) 650 °C for 3 h.

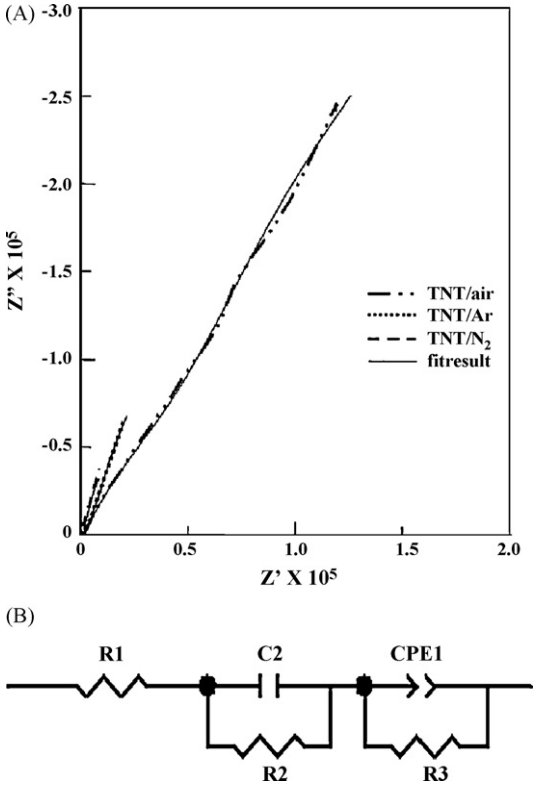

Fig. 3. EIS of TNT/air (dash-dot line), TNT/Ar (dot line) and TNT/N_2 (dash line) electrodes calcinated at 500 °C for 3 h and recorded at the potential of 0.1 V in 0.1 M Na_2SO_4. The solid line is the fitting curve. Plot B is the equivalent circuit used in the simulation.

3.2. EIS measurements

Electrochemical impedance spectroscopy, as a powerful technique widely used to study porous electrodes [27–29], was employed to investigate the electrical conductivity of the TNT arrays calcinated at 500 °C for 3 h in different gases. Fig. 3A presents the EIS spectra of TNT/air (dash dot line), TNT/Ar (dot line) and TNT/N_2 (dash line) electrodes recorded at the potential of 0.1 V in 0.1 M Na_2SO_4. An equivalent circuit $R_1(R_2C_2)(R_3$ CPE), shown in Fig. 3B, was often used to model the impedance data of porous material film according to the literature [30] and the solid line in Fig. 3A was the fitting curve. In this equivalent circuit, R_1 represents the uncompensated solution resistance; the parallel combination R_2C_2 is associated with the resistance and capacitance of the TiO_2 nanotube electrodes. The parallel combination of the charge transfer resistance (R_3) and the constant phase element (CPE) leads to a depressed semicircle in the corresponding Nyquist impedance plot [30]. All the fitting data was deduced directly using the electrochemical software *Z*-plot. The CPE is defined by CPE-T and CPE-P. In the present study, the fitting of the present data CPE-P results in 0.746, 0.739 and 0.734, respectively. Thus, the CPE-T values obtained in this work are close to capacitor C_{dl}. The parameters determined by the fitting of the experimental EIS data in the solution are summarized in Table 1. The resistance, R_2, of the TNT electrodes changed in the following order: $6.92 \times 10^5\ \Omega$ (TNT/air) > $3.95 \times 10^5\ \Omega$ (TNT/Ar) > $1.94 \times 10^5\ \Omega$ (TNT/N_2). The charge transfer resistance, R_3, decreased in the following order: $3.71 \times 10^5\ \Omega$ (TNT/air) > $1.15 \times 10^5\ \Omega$ (TNT/Ar) > $0.36 \times 10^5\ \Omega$ (TNT/N_2). These results showed that the TNT arrays calcinated in N_2 possesses higher electrical conductivity than that calcined in air and argon, or a factor of 3–10 enhancements.

Table 1
Impedance components for titania nanotubes electrodes calcinated at 500 °C for 3 h and determined by fitting EIS experimental data measured in 0.1 M Na_2SO_4 at 0.1 V using the equivalent circuit shown in Fig. 3B

Electrodes	R_1 (Ω)	R_2 ($\times 10^5$ Ω)	C_2 (μF)	R_3 ($\times 10^5$ Ω)	CPE-P	CPE-T (μF)
TNT/air	149	6.92	16.5	3.71	0.746	15.75
TNT/Ar	175	3.95	23.8	1.15	0.739	39.2
TNT/N_2	130	1.94	48.9	0.36	0.734	98.6

3.3. Electrochemical characteristics

The electrochemical properties of TNT electrodes annealed under different conditions were investigated by means of cyclic voltammetry with 10 mM $K_3[Fe(CN)_6]$ as an electrolyte in a potential range of −1.6 V to 2.0 V versus Ag/AgCl at a sweep rate of 0.1 V/s. Fig. 4 A is the CV results of TNT electrodes calcined in air, Ar and N_2 respectively at 500 °C for 3 h. TNT/air and TNT/Ar electrodes have oxidation peaks at 0.974 V and 1.209 V and reduction peaks at −0.343 V and −0.302 V. Their reduction–oxidation peak separation was approximately 1.317 V and 1.511 V. The large peak separation is attributed to the low electrical conductivity of the TiO_2 nanotube electrodes. This observation agrees well with the EIS data described in the previous section. It should be noted that as grown amorphous TNT electrode possessed only a reduction peak at −0.25 V, but no oxidation peak appeared at the reversed scan, which was ascribed to the further lower electrical conductivity. The solid line in Fig. 4A shows 20 cycles of CV results of TNT/N_2 electrode. TNT/N_2 electrode possesses a pair of well-defined oxidation/reduction peaks centered at 0.15 V and 0.31 V and the peak separation was 0.16 V. The peak current density equals to 1.35 mA, which suggested a quasi-reversible electrochemical reaction of $K_3[Fe(CN)_6]$. Except the first cycle, there is no appreciable change in the peak positions of both oxidation and reduction reactions, nor in the peak current density, which showed that the electrode reaction was very stable. The reduction and oxidation peaks can be ascribed respectively to the reduction and oxidation reactions of electroactive probe molecule, $K_3[Fe(CN)_6]$ on the TNT electrode surface. For less conductive electrode, it is difficult for electroactive probe molecules to lose electrons on the electrode surface, so the oxidation current density is lower than the reduction current density. Ghicov and co-authors also observed oxidation/reduction peaks for anatase π-TiO_2 tube electrode [31], but these peaks are ascribed to the intercalation and release of H^+ on the π-TiO_2 layer surface, which presented the oxidation of Ti^{3+} and reduction of Ti^{4+}. It is worthy further notice that their peak separation was of ∼0.3 V for annealed TiO_2 tubes, which is bigger than that in TNT/N_2 electrode (∼0.16 V). Fig. 4B compares the CV results of the TNT electrodes calcined in N_2 at 500 °C for different lengths of time. TNT/N_2 electrode annealed for 1 h possessed only a reduction peak, while no oxidation peak observed. This is similar to the CV curve measured in as-grown amorphous TNT arrays reported earlier [9] and thus suggests the low electrical conductivity. Although XRD revealed unambiguously the formation of anatase phase, it is possible that the anatase TiO_2 crystallites were dispersed in amorphous matrix or surrounded by thick amorphous grain boundaries. In this case, the electrical conductivity of the TNT arrays will be determined by the amorphous matrix or grain boundaries, as anatase TiO_2 nanocrystallites did not form a percolated network for charge transfer. That would explain well the fact that the CV curve of TNT/N_2 arrays is almost identical to that of as-grown amorphous TNT electrode. TNT/N_2 electrode annealed for 6 hrs demonstrated well-defined oxidation/reduction peaks, similar to that observed in TNT/N_2 electrode annealed for 3 h. However, the peak separation voltage 0.5 V is greater as compared to 0.16 V in 3 h annealing TNT. The peak current densities were also much lower, 0.57 mA and 0.75 mA, than that of 3 h annealing TNT electrode (1.35 mA). The change of the electrochemical properties may be attributed to the difference in both microstructure and crystallinity. TNT arrays partially collapsed when annealed for 6 h with much reduced surface area and the formation of rutile TiO_2 phase occurred judging from SEM and XRD analyses. Reduced surface area would result in a lower current density, while the presence of rutile phase may lead to an increased electrical resistance and thus an increased peak separation voltage.

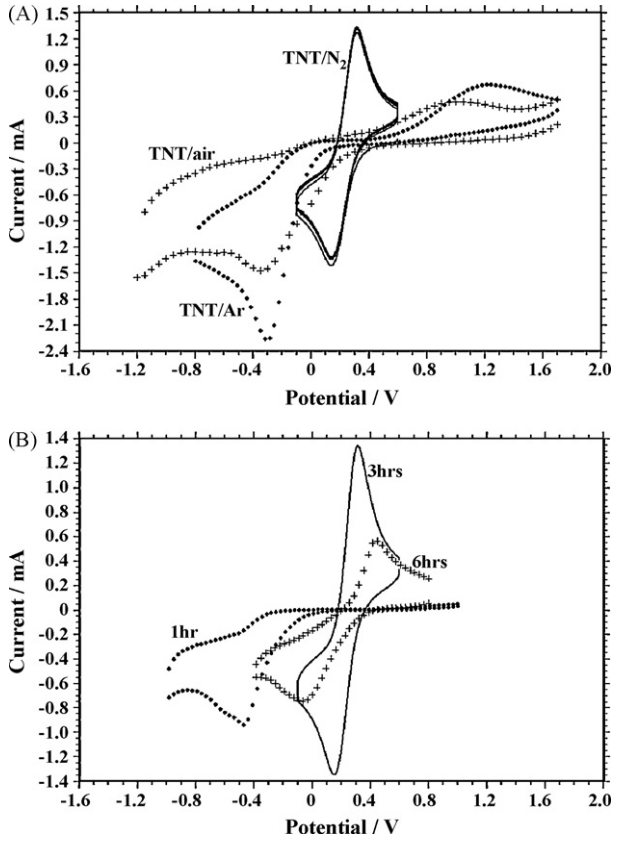

Fig. 4. Cyclic voltammetry of 10 mM $K_3[Fe(CN)_6]$ with (A) TNT/air (cross line) and TNT/Ar (dot line) and TNT/N_2 of 20 cycles (solid line) calcined at 500 °C for 3 h; (B) TNT/N_2 electrodes calcined at 500 °C for 1 h (dot line), 3 h (solid line) and 6 h (cross line).

Some significant information about the electron transport in TiO_2 nanotubes calcined in different gases can be obtained from photocurrent measurements. Fig. 5A compares photocurrent of TNT electrodes calcined in air, Ar and N_2 respectively at 500 °C for 3 h under UV radiation in the range of 366 nm at a potential of 1.5 V (Ag/AgCl). As-grown amorphous TNT electrode shows a negligible photocurrent density of ∼2.0 mA cm^{-2}; however, TNT electrodes calcined in air and argon, demonstrated photocurrent densities increasing to 34 mA cm^{-2} and 64 mA cm^{-2}, respectively. TNT/N_2 electrode had the highest photocurrent density of 84 mA cm^{-2}. The photocurrent density corroborates with the EIS and CV measurements described in the previous paragraphs. The high photocurrent density is directly related to the electrical conductivity of the TNT arrays. The as-grown amorphous TNT arrays have the highest electrical resistance; whereas the TNT/N_2 arrays have the lowest electrical resistance. The photocurrent density in TNT/N_2 and TNT/Ar electrodes are 147% and 90% higher than that of TNT/air electrodes. The significant increase in photocurrent density in TNT electrodes calcined at 500 °C for 3 h, as compared to as-grown amorphous TNT electrode indicated the necessity to form anatase phase for such photoelectrical response, which is obviously related

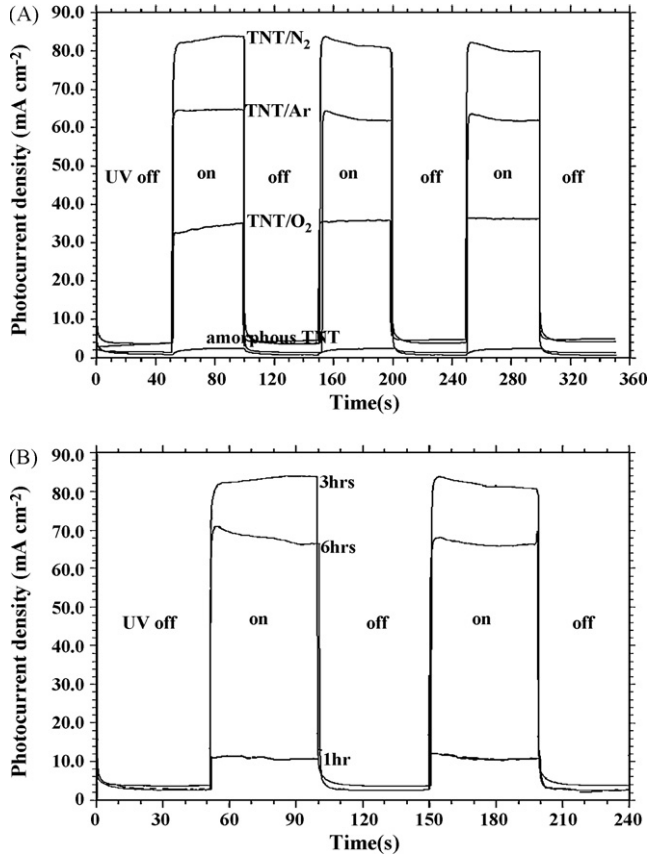

Fig. 5. Photocurrent response of: (A) TNT electrodes calcined in different gas at 500 °C for 3 h; (B) TNT/N_2 electrodes calcined for different hours.

to the band gap, 3.2 eV, of anatase TiO_2. Fig. 5B shows the photocurrent density of TNT/N_2 electrodes calcinated for various length of time. TNT/N_2 electrode annealed for 1 h has a rather low photocurrent density of ~7.0 mA cm^{-2}, similar to that of as-grown amorphous TNT arrays. Such a similarity in lower photocurrent density further suggests the hypothesis that anatase TiO_2 nanocrystallites are likely dispersed in amorphous matrix or surrounded by thick amorphous grain boundaries, and did not form a percolated network for charge transfer. TNT/N_2 electrodes annealed for 6 h has a photocurrent density of ~66 mA cm^{-2}, less than that of TNT/N_2 electrode annealed for 3 h. Such a reduction of photocurrent density is in a good agreement with CV measurements and is ascribed to the partial collapse of nanotube structures. Ghicov also reported the increase of photocurrent conversion efficiencies for TiO_2 nanotubes annealed in air or dry Ar for 1 h [32], according to their experiment, the photocurrent for the Ar annealed samples is less than the samples annealed in air, this result was different with us because the annealing time is different.

There are two possible effects on TNT arrays when annealed in nitrogen. One is nitrogen doping in TNT arrays through substitution of oxygen in anatase with nitrogen as reported in literature [22]. Considering the experimental conditions used in the current study, the annealing temperature below 500 °C in dry nitrogen without any catalyst, nitrogen doping is very unlikely as the nitrogen molecules with triple chemical bonds are very stable. Another possible effect is the partial reduction of tetravalent titanium cations. Some literatures have reported the change of the band gap of TiO_2 due to the reduction of Ti^{4+}, for example, Macak selectively switched on the pore bottoms by reductive self-doping of TiO_2 nanotube with Ti^{3+} and established a sufficient conductivity contrast to allow Cu deposition [33]. Guillemot demonstrated that low-temperature vacuum annealing can create a controlled number of Ti^{3+} defects [34]. Change of electrical properties of oxides through thermal annealing under various gases is also well established in literature [35]. Annealing under a reductive environment, such as in nitrogen, are likely to result in reduction of part of Ti^{4+} cations to lower valence state. At the same time, defects, such as the oxygen vacancies, can be generated in the TiO_2 structure due to a partial oxygen loss [32]. That in turn would change the electron density and the electrical properties of the material. The EIS results combined with the color change strongly indicates this change. Such impact would become more significant in nanostructured materials due to the huge surface to volume ratio. Consequently a higher photocurrent density was observed in TNT arrays annealed in nitrogen.

4. Summary

Crystallized titania nanotubes arrays have been successfully prepared by anodic oxidation of titanium foil followed with calcination in different gases. Calcination at temperatures ranging from 300 to 650 °C resulted in a change of TiO_2 from amorphous to anatase to rutile phase and a change of morphology, i.e. reduction in inner diameter and increase in wall thickness at the expense of nanotube length. High temperature and prolonged annealing time led to the collapse of nanotube array structure. Annealing in dry nitrogen at 500 °C for 3 h appeared to be the most favorable conditions to retain desired nanotube array structure with desirable anatase phase and electrochemical and photoelectrical properties. Partial reduction of tetravalent titanium cations and the formation of oxygen vacancies were ascribed to explain the change of the electrochemical and photoelectrical properties of the TiO_2 nanotube arrays.

Acknowledgements

P. Xiao gratefully acknowledges the fellowship from the Chinese Scholarship Council and the supporting of Science Foundation of Chongqing Science and Technology Committee (CSTS, 2007BB4157), and this work is supported in part by National Science Foundation (DMI-0455994) and Air Force Office of Scientific Research (AFOSR-MURI, FA9550-06-1-032).

References

[1] D. Gong, C.A. Grimes, O.K. Varghese, W. Hu, R.S. Singh, Z. Chen, E.C. Dickey, J. Mater. Res. 16 (2001) 3331–3334.
[2] A. Ghicov, H. Tsuchiya, J.M. Macak, P. Schmuki, Electrochem. Commun. 7 (2005) 505–509.
[3] Q. Chen, W. Zhou, G. Du, L.M. Peng, Adv. Mater. 14 (2002) 1208–1211.
[4] T. Peng, A. Hasegawa, J. Qin, K. Hirao, Chem. Mater. 15 (2003) 2011–2016.
[5] O.K. Varghese, D. Gong, M. Paulose, K.G. Ong, C.A. Grimes, Sens. Actuators B: Chem. 93 (2003) 338–344.
[6] D.V. Bavykin, E.V. Milsom, F. Marken, D.H. Kim, D.H. Marsh, D.J. Riley, F.C. Walsh, K.H. El-Abiary, A.A. Lapkin, Electrochem. Commun. 7 (2005) 1050–1058.
[7] H. Tsuchiya, J.M. Macak, L. Müller, J. Kunze, F. Müller, P. Greil, S. Virtanen, P. Schmuki, J. Biomed. Mater. Res. 77A (2006) 534–541.
[8] J.M. Macak, H. Tsuchiya, L. Taveira, A. Ghicov, P. Schmuki, J. Biomed. Mater. Res. 75A (2005) 928–933.
[9] P. Xiao, B.B. Garcia, Q. Guo, D.W. Liu, G.Z. Cao, Electrochem. Commun. 9 (2007) 2441–2447.
[10] M.S. Sander, M.J. Côté, W. Gu, B.M. Kile, C.P. Tripp, Adv. Mater. 16 (2004) 2052–2057.
[11] A. Michailowski, D. AlMawlawi, G.S. Cheng, M. Moskovits, Chem. Phys. Lett. 349 (2001) 1–5.
[12] Q. Chem, W.Z. Zhou, G.H. Du, L.H. Peng, Adv. Mater. 14 (2002) 1208–1211.
[13] J.M. Macák, H. Tsuchiya, P. Schmuki, Angew. Chem. Int. Ed. 44 (2005) 2100–2102.
[14] S. Liu, A. Chen, Langmuir 21 (2005) 8409–8413.
[15] E. Topoglidis, C.J. Campbell, A.E.G. Cass, J.R. Durrant, Langmuir 17 (2001) 7899–7906.
[16] R.P. Vitiello, J.M. Macak, A. Ghicov, H. Tsuchiya, L.F.P. Dick, P. Schmuki, Electrochem. Commun. 8 (2006) 544–548.

[17] A. Ghicov, J.M. Macak, H. Tsuchiya, J. Kunze, V. Haeublein, L. Frey, P. Schmuki, Nano Lett. 6 (2006) 1080–1082.
[18] G.K. Mor, O.K. Varghese, M. Paulose, K. Shankar, C.A. Grimes, Sol. Energy Mater. Sol. Cells 90 (2006) 2011–2075.
[19] K. Noworyta, J. Augustynski, Solid State Lett. 7 (2004) E31–E33.
[20] Y. Xie, Electrochim. Acta 51 (2006) 3399–3406.
[21] Q. Cai, M. Paulose, O.K. Varghese, C.A. Grimes, J. Mater. Res. 20 (2005) 230–236.
[22] T. Ma, M. Akiyama, E. Abe, I. Imai, Nano Lett. 5 (2005) 2543–2547.
[23] G.Z. Cao, Nanostructures & Nanomaterials, Imperial College Press, London, 2004, p. 224.
[24] J.S. Reed, Principles of Ceramics Processing, 2nd edn., Wiley, New York, 1995, p. 173.
[25] O.K. Varghese, D. Gong, M. Paulose, C.A. Grimes, E.C. Dickey, J. Mater. Res. 18 (2003) 156–165.
[26] R. Beranek, H. Tsuchiya, T. Sugishima, J.M. Macak, L. Taveira, S. Fujimoto, H. Kisch, P. Schmukic, Appl. Phys. Lett. 87 (2005), 243114-1–243114-3.
[27] A. Chen, S. Nigro, J. Phys. Chem. B 107 (2003) 13341–13348.
[28] S. Carrara, V. Bavastrello, D. Ricci, E. Stura, C. Nicolini, Sens. Actuators B: Chem. 109 (2005) 221–226.
[29] M. Wang, L. Wang, G. Wang, X. Ji, Y. Bai, T. Li, S. Gong, J.H. Li, Biosens. Bioelectron. 19 (2004) 575–582.
[30] L.A. da Silva, V.A. Alves, M.A. da Silva, S. Trasatti, J.F.C. Boodtst, Electrochim. Acta 42 (1997) 271–281.
[31] A. Ghicov, H. Tsuchiya, R. Hahn, J.M. Macak, A.G. Muñoz, P. Schmuki, Electrochem. Commun. 8 (2006) 528–532.
[32] A. Ghicov, H. Tsuchiya, J.M. Macak, P. Schmuki, Phys. Stat. Sol. (a) 203 (2006) R28–R30.
[33] J.M. Macak, B.G. Gong, M. Hueppe, P. Schmuki, Adv. Mater. 19 (2007) 3027–3031.
[34] F. Guillemot, M.C. Porté, C. Labrugère, Ch. Baquey, J. Colloid Interf. Sci. 255 (2002) 75–78.
[35] V. Vaithianathan, S. Hishita, J.H. Moon, S.S. Kim, Thin Solid Films 515 (2007) 6927–6930.

Biographies

Peng Xiao is completing her PhD studies at the Chongqing University, China, in the area of condense matter physics. She was awarded a scholarship from CSC in 2006 and studied in MSE department at the University of Washington as a visiting scholar. Her interests include synthesis of nanomaterials and matrixes for biosensor/immuno sensor applications.

Dawei Liu is studying for his PhD in MSE department, University of Washington, his research interest is intercalation properties of lithium battery cathode.

Betzaida Batalla Garcia is studying for her PhD in MSE department, University of Washington, her research focus on meso-microporous sol–gel derived carbon cryogels for energy storage applications and electrochemical impedance spectroscopy.

Saghar Sepehri is currently working on PhD in MSE department, University of Washington, her research focus on microporous carbon cryogels for hydrogen storage.

Yunhuai Zhang is a professor in Department of Chemical Engineering, Chongqing University, PR China. He is now studying in MSE Department at the University of Washington as a visiting scholar. His research interest is synthesis of nanomaterials and characterization.

Guozhong Cao held a PhD on ceramics materials from Eindhoven University of Technology, Netherlands in 1991. He is a professor in Department of Materials Science and Engineering at the University of Washington and takes a particular interest in synthesis nanomaterials, electrochemical batteries, supercapacitors and nanostructured oxides for solar cells.